NUCL SCI TECH (2021)32:79
https://doi.org/10.1007/s41365-021-00917-8

Performance of digital data acquisition system in gamma-ray spectroscopy

Di-Wen Luo[1] · Hong-Yi Wu [1] · Zhi-Huan Li[1] · Chuan Xu[1] · Hui Hua[1] · Xiang-Qing Li[1] · Xiang Wang[1] · Shuang-Quan Zhang[1] · Zhi-Qiang Chen[1] · Chen-Guang Wu[1] · Yu Jin[1] · Jie Lin[1]

Received: 22 April 2021 / Revised: 6 June 2021 / Accepted: 11 June 2021

Abstract A newly developed digital data acquisition system, which is based on the digital pulse processor Pixie-16 modules by XIA LLC, was tested with the γ-ray detector array of the China Institute of Atomic Energy using the γ-ray source and in-beam γ-rays. A comparison between this digital data acquisition system and the conventional analog data acquisition system was made. At a low count rate, both systems exhibit good and comparable energy resolutions. At a high count rate above 8.8 k/s, while the energy resolution obtained by the analog system deteriorates significantly, the energy resolution obtained by the digital system is nearly unchanged. Meanwhile, experimental data with higher statistics can be collected by the digital system. The advantage of this digital system over the conventional analog system can be ascribed to its excellent capability of handling pile-up pulses at higher count rates, and the fact that it has nearly no dead time in data transmission and conversion.

Keywords Digital data acquisition system · Gamma spectroscopy · Energy resolution

This work was supported by the National Key R&D Program of China (No. 2018YFA0404403), the National Natural Science Foundation of China (Nos. 12035001, 12075006, 11675003), and the State Key Laboratory of Nuclear Physics and Technology, PKU (No. NPT2020KFY18).

✉ Zhi-Huan Li
zhli@pku.edu.cn

✉ Hui Hua
hhua@pku.edu.cn

[1] State Key Laboratory of Nuclear Physics and Technology, School of Physics, Peking University, Beijing 100871, China

1 Introduction

The large Compton-suppressed high-purity germanium (HPGe) detector array is one of the most powerful tools for obtaining spectroscopic information about the structure of atomic nuclei [1, 2]. The traditional analog data acquisition system (ADAQ) has been widely used to match these HPGe detectors, i.e., after the preamplifier stage, signals from detectors are processed in electronic modules like shaping amplifiers, discriminators, analog-to-digital converters (ADCs), time-to-digital converters (TDC), etc., and finally stored for offline analysis. Recently, the digital data acquisition system (DDAQ) has been developed and is overtaking the conventional ADAQ in gamma spectroscopy. The basic principle of the DDAQ is that the output pulse profile of the preamplifier is digitized immediately, and various algorithms replace the functions of analog shaping and timing electronic units to extract spectroscopic information from the pulse.

Owing to much higher pulse processing flexibility, the DDAQ has demonstrated significant advantages over the conventional ADAQ [3–8]. In the application of detectors in environments with high γ-ray count rates, pulse pile-up that distorts the energy spectra becomes a non-negligible issue. In the conventional ADAQ, pile-up events are discarded to get high-resolution spectra. The detection efficiency thus decreases. In particular, the capability of the ADAQ is limited in measurements where the signal rate of the nuclei of interest is low, while the signal rate of the accompanying contaminant nuclei is high. With the proper algorithms adopted in the DDAQ, the pile-up pulses can be effectively disentangled rather than rejected, and all the information carried by the overlapping pulses can be precisely recorded. With the capability to restore the original

Published online: 04 August 2021

information of the detector pulses, the DDAQ has been successfully implemented in many recent γ-ray detector arrays, such as TIGRESS [9, 10], GRETA [11, 12], SeGA [13, 14], AGATA [15, 16], and INGA [17, 18].

A flexible DDAQ, developed recently at Peking University [19], has been successfully applied and verified in γ-spectroscopy experiments at the China Institute of Atomic Energy (CIAE) and iThemba LABS in South Africa. Here, the performance measurements of this DDAQ with the γ-ray detector array of the CIAE are presented in comparison with those of the conventional ADAQ. The paper is organized as follows: Sect. 2 describes the data acquisition system, Sects. 3 and 4 present the measurements with γ-ray sources and in-beam γ-rays, respectively, and a summary is given in Sect. 5.

2 Basic feature of data acquisition systems

The γ-ray detector array of CIAE [20] consisted of six HPGe detectors with bismuth germinate (BGO) anti-Compton suppressors, two clover detectors, and two planar HPGe detectors. The relative efficiencies for one HPGe detector and one clover detector are around 30% and 40%, respectively. To compare the performance between the DDAQ and ADAQ, each output channel of the detectors was preamplified and divided into two channels with a divider. One was sent to the conventional ADAQ and the other was sent to the DDAQ.

As shown in Fig. 1a, the ADAQ consisted of timing filter amplifiers (TFA), shaping amplifiers, constant fraction discriminators (CFD), pulse stretchers, ADCs, TDCs, fast trigger modules, etc. The signals from the detectors include timing signals and energy signals. The timing signals from the HPGe detectors and BGO Compton Shields were successively sent to TFA and CFD. The CFD output signals from the HPGe detectors were first vetoed with the signals from the respective Compton-suppressed BGO and then sent to the multiplicity trigger logic units, where the master trigger was produced within a user-defined coincidence window. The trigger signal was used to produce the ADC and TDC gates. The CFD output signals were also sent to the TDC. The energy signals from the HPGe detectors were first processed by a shaping amplifier and then sent to the ADC. After conversion, the energy and time information of an event were stored in a computer for later analysis. In the measurements, the parameters of conventional modules in ADAQ, such as the gain of the amplifier, shaping time constant, stretching time, delay time, and trigger setup, were carefully adjusted.

The DDAQ used in the measurements was composed of 16-channel Pixie-16 modules and one controller. The principal components of this DDAQ were mainly manufactured by XIA LLC [21]:

(A) Pixie-16 6U CompactPCI/PXI chassis.
(B) PCI-8366/PXI-8368, chassis controller.
(C) Pixie-16, 12/14/16 bits, 100/250/500 MSPS ADC.
(D) Pixie-16 MicroZed-based Trigger I/O (MZTIO), a programmable trigger module.
(E) Pixie-16 clock and trigger rear I/O module.

Signals from the detectors are digitized by the Pixie-16 ADC modules. The Pixie-16 chassis based on CompactPCI/PXI standards allows experimental data transfer from module memories to the host computer at a rate of up to 109 MByte/s, while the system communication and control occur through the PCI-8366/PXI-8368 chassis controller. For an extensible DDAQ, synchronization of the clock and distribution of triggers between separate chassis is provided by the Pixie-16 clock and trigger rear I/O module, which can synchronize up to a maximum of eight chassis (1600 channels). In addition, timestamps provide absolute timing information to event data and allow the use of individual triggers for separate data acquisition (DAQ) systems. Detailed information on the technical implementation, including synchronization of the clock and distribution of triggers between separate chassis, can be found in Refs. [22, 23]. The MZTIO is designed to route signals between the PXI backplane and the chassis front panel and make logical combinations between them in a field-programmable gate array (FPGA) fabric. A timestamp provides absolute timing information to event data and allows the use of individual triggers for separate data acquisition systems.

The DDAQ applied to the measurements is shown in Fig. 1b, where the data flowing through different parts of the Pixie-16 module are illustrated. The output of the preamplifier is directly digitized by the Pixie-16 ADC module. Then, the data stream is fed into two branches. One goes through the fast filter to produce fast triggers, which are sent to the system FPGA. A delay FIFO is used to compensate for the delay between the fast triggers and external triggers. After passing through an external delay, the other one is divided into three parts: (1) an energy filter for peak height sampling, (2) a pile-up detector, and (3) CFD circuitry in which a trigger is generated to latch timestamps and record traces. The control logic utilizes the veto stretched signal latched by the system FPGA and/or the external triggers to determine whether and when to stream waveform data into the trace dual port memory (DPM) and write event information into the header DPM. A photograph of the DDAQ is shown in Fig. 1c.

In the DDAQ, all parameters were adjusted on the software interface with dedicated algorithms based on digital signal processing (DSP). The trigger system of the

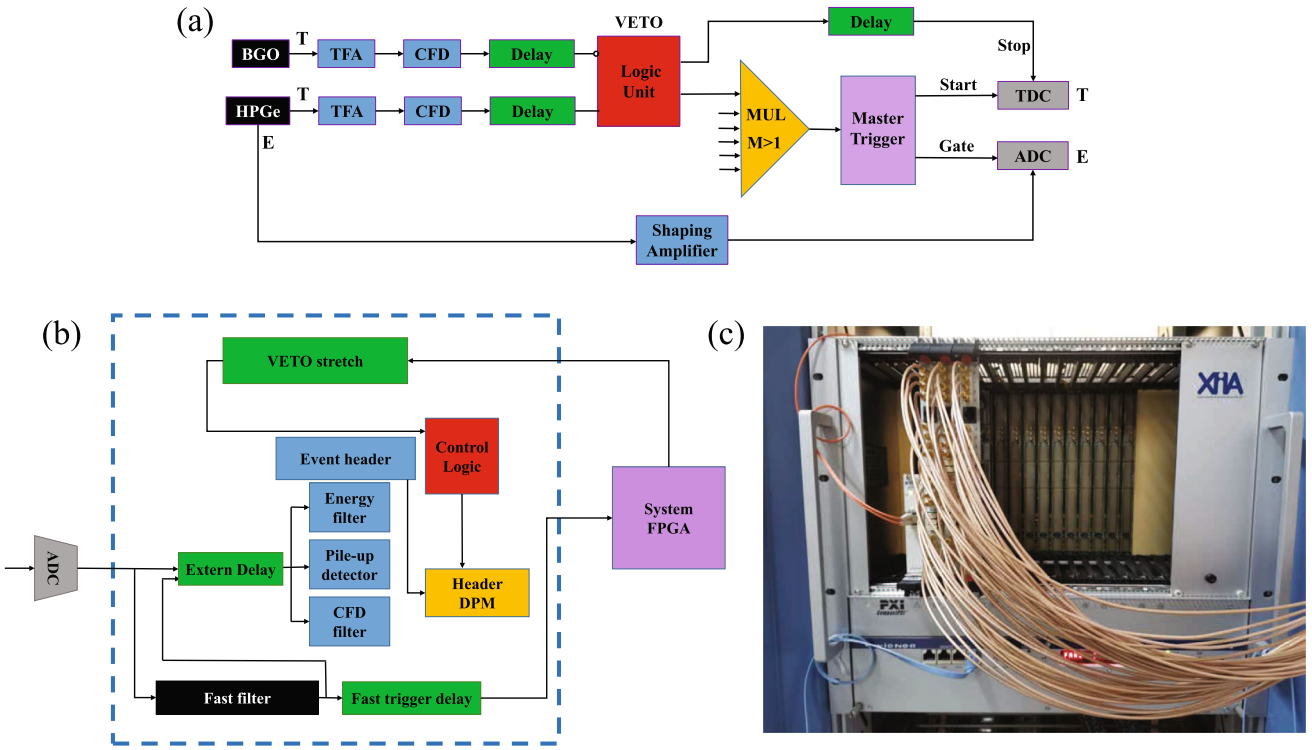

Fig. 1 (Color online) **a** Diagram of ADAQ in gamma-ray spectroscopy. **b** Diagram of the DDAQ in gamma-ray spectroscopy. **c** Photograph of the DDAQ

DDAQ consisted of two interdependent parts: an internal trigger and an external trigger. For the internal trigger, a threshold was preset to the Pixie-16 modules. If output signals from the preamplifier/PMT crossed the threshold, fast trigger pulses were generated in the signal processing FPGA and sent to the system FPGA. The user-selectable "control logic," which includes module/channel validation triggers, vetoes, etc., decides whether the corresponding event is recorded or not. The multiplicity and/or coincidence in each Pixie-16 module or between Pixie-16 modules was performed in the system FPGA.

For an external trigger, a programmable MZTIO module was developed to implement efficient and flexible trigger patterns. The MZTIO module is based on a custom carrier board and a commercial MicroZed Zynq processor module, which combines the FPGA fabric (for the trigger logic) and an ARM processor (running Linux) on the same chip. All Zynq firmware and software were customized for the DDAQ. The external triggering mechanism was implemented as follows: the multiplicity triggers were generated for each selected channel in the immediately neighboring Pixie-16 modules and sent to the low-voltage differential signaling (LVDS) inputs of the MZTIO, where the corresponding trigger signal was generated according to user-customized logic and then sent back as a module validation trigger of the Pixie-16 modules. An example of trigger generation can be found in Ref. [19]. To make it easy to incorporate various types of logic in MZTIO, some basic functions such as "Delay", "Scaler", and "Coincidence" were also developed for the DDAQ. In addition, Pixie-16 module signals (delayed local fast trigger, stretched module/channel validation trigger, and stretched veto trigger) could be monitored by the MZTIO through the chassis backplane.

With the powerful trigger logic system of the DDAQ, the complex logic operation of time signals from different detectors can be easily realized. Here, taking the BGO anti-coincidence as an example, the timing diagram of the trigger for BGO anti-coincidence is shown in Fig. 2a. It can be seen that when the γ-rays are detected by the HPGe detector and the surrounding BGO detectors simultaneously, and the signal of HPGe detector falls into the signal range of the BGO detectors, the first HPGe signal is vetoed. Without the stretched BGO veto signal, the second HPGe trigger is validated. Its timestamp is latched, and the corresponding event header information is written. Through the digital I/O port in the Pixie-16 module, the timing relationship between the HPGe and BGO signals can also be easily monitored by the oscilloscope (shown in Fig. 2b). Based on the observed timing relationships, the delay and width of the trigger signals can be adjusted.

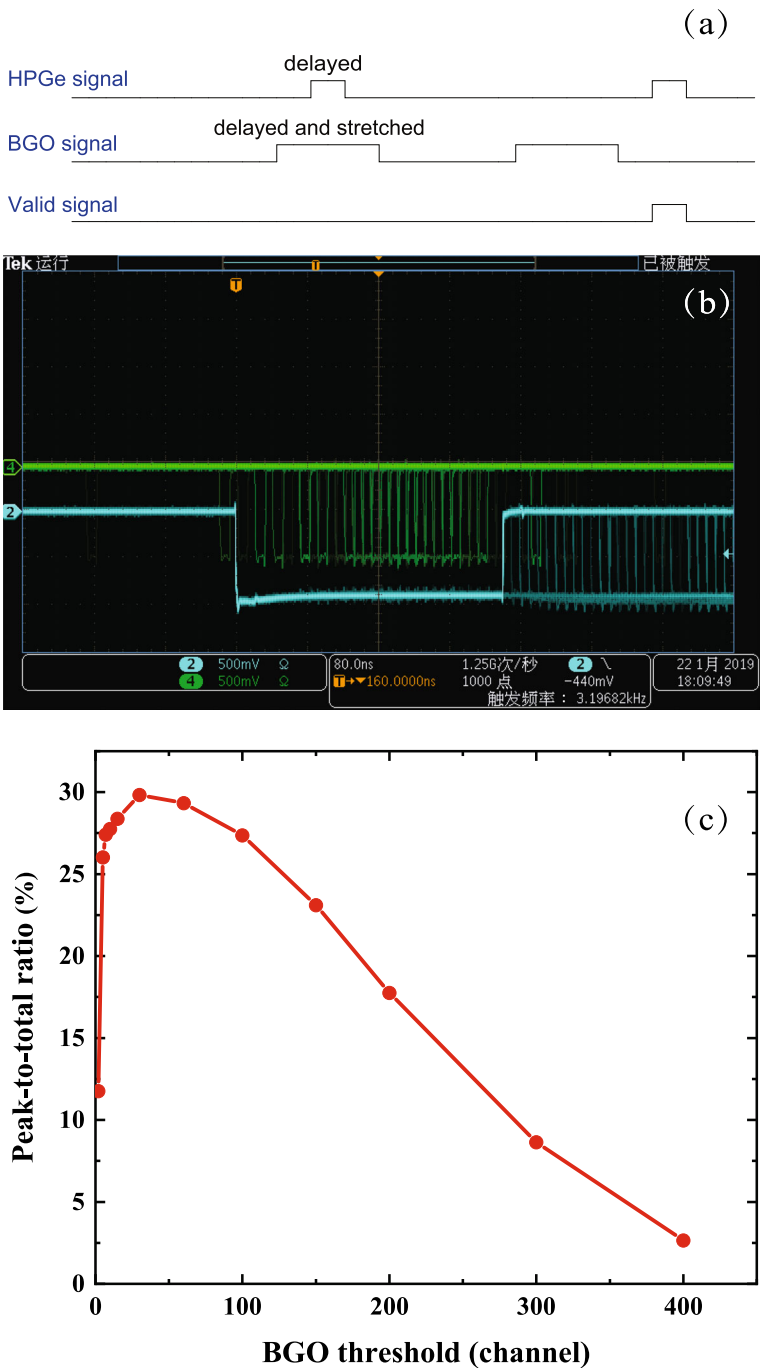

Fig. 2 (Color online) **a** Timing diagram for BGO anti-coincidence; **b** Timing relationship between the HPGe and BGO signals monitored by the oscilloscope. The HPGe and BGO signals are shown in green and blue, respectively. **c** The peak-to-total ratio of the HPGe detector as a function of the BGO threshold for the DDAQ

3 Measurements with γ-ray sources

In γ-ray spectroscopy, to get a high-quality spectrum, a high peak-to-total ratio (P/T) is crucial. In the present measurements, the P/T of the HPGe detector, which is defined as the ratio of the sum of peak counts (1173.2- and 1332.5-keV γ-rays of ^{60}Co source) to the total counts in the energy range between 30 and 1350 keV, is shown as a function of the BGO threshold for the DDAQ in Fig. 2c. It can be seen that when the BGO threshold is around 40 channel (ch), the P/T has a maximum value. Also, there is a relatively flat peak in the P/T curve near the maximum value, i.e., the P/T value changes little in the BGO threshold range of 40–80 ch. To improve the noise immunity of the system, generally, the BGO threshold is not directly selected as the value with the maximum P/T, but a slightly larger value. In this way, if the noise of the BGO detector increases slightly during the measurements, a good anti-Compton effect can still be guaranteed. Similarly, the anti-Compton optimization of the ADAQ was

also carried out in this work, and the results were close to those of the DDAQ.

With the optimized trigger mechanism and the carefully chosen BGO threshold, the ADAQ and DDAQ can exhibit good and comparable energy resolutions in measurements with γ-ray sources. Both the energy resolutions of the HPGe detectors for the 1332.5-keV γ-ray of the ^{60}Co source obtained by the ADAQ and DDAQ are around 2.0–2.5 keV.

4 Measurements with in-beam γ-rays

Measurements with in-beam γ-rays were performed at the HI-13 tandem facility of the CIAE. The energy of the ^{12}C beam was 67 MeV. By bombarding the 0.98 mg/cm^2 ^{54}Cr target with a 10.6 mg/cm^2 ^{197}Au backing, the high-spin states of nuclei of interest were populated via the fusion–evaporation reactions. The parameter setup of modules in the ADAQ in the in-beam measurements was the same as that in the γ-ray source measurements. For the ADAQ, a valid event required at least twofold γ–γ coincidence ($M \geq 2$).

Compared with the measurements with γ-ray sources, the in-beam measurements are normally performed in an environment with more noise. There are typically two main noise sources: (1) electronic noise in the system and (2) detector signals from the deexcitation of surrounding beam-activated products. The noise causes a serious disturbance to the γ-ray spectrum. First, the solution for electronic noise will be discussed here, and the solution of random coincidence events from surrounding beam-activated products will be discussed in the following in combination with the in-beam coincident spectrum.

To minimize the interference of electronic noise, a reasonable trigger is important for in-beam measurements. In the ADAQ, a timing filter amplifier (such as the ORTEC 474 module) is usually used for fast time shaping. However, the integral and differential time constants of the module can only be selected by six gears with large intervals, which cannot be adjusted continuously. The fast time signal after shaping is sent to the CFD. However, the capacitance in CFD at the zero-crossing point needs a certain amount of charge accumulation to make the output signal change from 0 to 1, so the trigger does not occur when the small signals do not meet the above conditions. In addition, when the signal-to-noise ratio is poor, a zero-crossing point cannot be produced. Therefore, although the threshold of CFD can be set as low as possible, for small pulses or poor signal-to-noise ratios, their triggering efficiencies are still low.

In the DDAQ, as shown in Fig. 1a, the trigger of the pulse is generated by a fast filter. The fast filter differentiates the pulse signal to get the trigger signal after running the average of the input pulse [24]. With the fast filter, the signal-to-noise ratio of the trigger signal is significantly improved, so a very low trigger threshold can be selected to achieve a high triggering efficiency for signals with small amplitudes. Moreover, the digital filter parameters can be adjusted continuously within a certain range, so the optimal parameters are easily selected to get the maximum signal-to-noise ratio. Compared with the CFD discrimination in the ADAQ, the time resolution of the trigger signal after the fast filter in the DDAQ is a little worse. However, since the digital system is timestamp based, as shown in Fig. 1a, the CFD filter and fast filter are independent. The CFD filter performs constant fraction timing discrimination only when the fast filter generates trigger logic. If the CFD filter finds a zero-crossing point, the event's timestamp is generated by the CFD filter. Otherwise, the timestamp is provided by the fast filter threshold crossing time. Therefore, the high-resolution time information of the signal triggered by CFD is not lost, and the small signals triggered by the fast filter are also recorded, which ensures a high triggering efficiency for small signals.

To get sufficient data for statistical analysis in the in-beam measurements, the DDAQ was operated with a triggerless mode, which allows each channel to record all live events individually regardless of the selection of event multiplicity. This mode provides great flexibility for offline data analysis. The raw data streams included the timestamp of the event for the time correlation offline analysis. In the in-beam measurements, a total of 4.76×10^8 twofold and higher γ-ray coincidence events were collected by the DDAQ, which is almost twice the total 2.35×10^8 twofold and higher-fold γ-ray coincidence events collected by the ADAQ under the same experimental conditions.

It is known that high γ-ray count rates in detectors usually lead to serious pulse pile-up and distort the energy spectra. As mentioned above, the common solution in the conventional ADAQ is to discard the events that are badly distorted owing to pile-up. This approach leads to a decrease in counting efficiency. When pile-up signals constitute a large fraction of the detected events, this approach is not suitable owing to the intolerable counting loss. An alternate approach is to reduce the filter time constants of pulse-shaping modules, which makes the output signals as short as possible to diminish the pile-up events. This will result in a worsening of the energy resolution. Furthermore, because some signals have serious overlaps at high counting rates, the distortion of the pulse height cannot be totally eliminated, and high-quality

spectra are thus not available in the high counting rate environment for the ADAQ.

For the DDAQ, with the proper algorithms, the pile-up pulses can be disentangled effectively. As an example, Fig. 3 illustrates how the pile-up signal is processed by the DDAQ and ADAQ. Three typical pulse signals from the preamplifier output with equal amplitude and short rise time, followed by a long exponential tail (shown in Fig. 3a), among which the second and third signals are seriously piled up, are input to the ADAQ and DDAQ. In the ADAQ, the input signal is first shaped into a Gaussian signal, which has a long tail, as shown in Fig. 3b. The peak height of the Gaussian shaping signal represents the energy of the event. Since the peak-sensitive ADC of the ADAQ looks for the maximum value of the Gaussian shaping signal in the acquisition gate, the energy information of the first pulse in Fig. 3b can be accurately obtained using the ADAQ. However, as shown in Fig. 3b, because of the overlapping of the second and third Gaussian shaping signals, the height of the rising edge of the third signal is higher than the peak height of the second signal in the acquisition gate. Consequently, the true amplitude of the second pulse cannot be acquired. Furthermore, the third pulse is not recorded by the ADAQ because of the dead time of the system. Therefore, only the first input signal is recorded effectively by the ADAQ.

In DDAQ, the triangular [25] and trapezoidal [26] pulse-shaping algorithms have been widely adopted. Their filter functions decay back to the baseline very quickly. In this example, the trapezoidal pulse-shaping algorithm, whose rise time is equal to its fall time, is used. As shown in Fig. 3b, when the interval between two neighboring pulses is larger than the sum of the rising time and flat time of the trapezoidal signal, the superimposed pulse can be correctly processed by the trapezoidal algorithm. Consequently, the effects of pile-up are removed without discarding distorted events. In addition to the first input signal, both the energy information of the second and third input signals are precisely recorded by the DDAQ.

In the in-beam measurements, the performances of the ADAQ and DDAQ at different counting rates were tested and compared. Figure 4 shows the energy resolutions of the HPGe detector for the 925.1-keV γ-ray of ^{62}Cu obtained by the ADAQ and DDAQ as functions of the count rate in the HPGe detector. It can be seen that at low count rates, both data acquisition systems have similar energy resolutions. At high count rates above 8.8 k/s, where the pile-up becomes serious, the energy resolution obtained by the ADAQ deteriorates significantly, while the energy resolution obtained by the DDAQ is nearly unchanged.

Based on at least twofold γ–γ coincidence, Fig. 5 shows the typical energy spectra of an HPGe detector measured by the ADAQ and DDAQ within the same time range at count rates of 3.1 and 8.8 k/s. It can be seen in Fig. 5a that at a low count rate of 3.1 k/s, both spectra by the ADAQ and DDAQ show similar energy resolutions, and the DDAQ has higher data throughput. The ADAQ used in the measurements was based on the Versa Module Eurocard (VME) bus. Generally, it takes a dozen to tens of microseconds for the front-end module in VME to acquire an event and wait for the readout to transfer it, which will

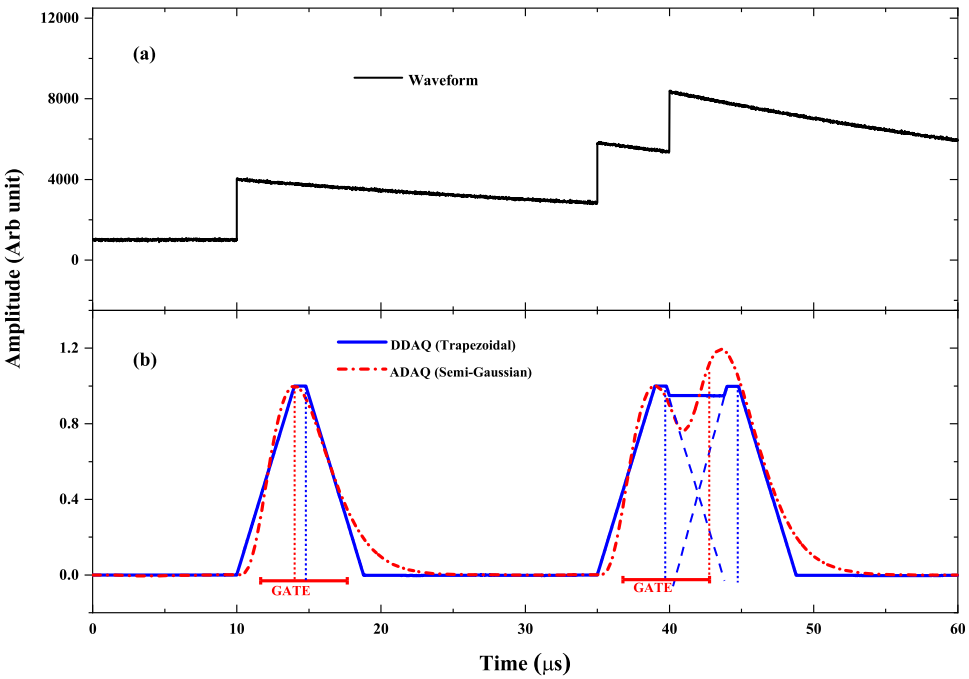

Fig. 3 (Color online) **a** Input pulse signals with equal amplitude. **b** Pulse processing in the ADAQ and DDAQ. The vertical dotted lines show the positions where the amplitudes of the pulses were sampled by the ADAQ and DDAQ

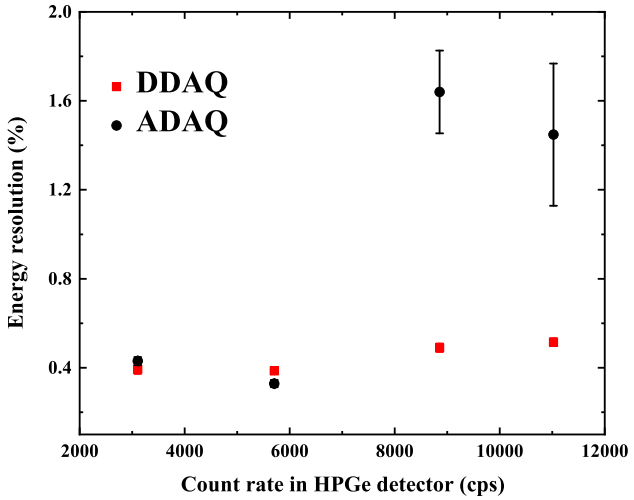

Fig. 4 (Color online) Energy resolutions of HPGe detector obtained by the ADAQ and DDAQ as functions of count rate in the HPGe detector

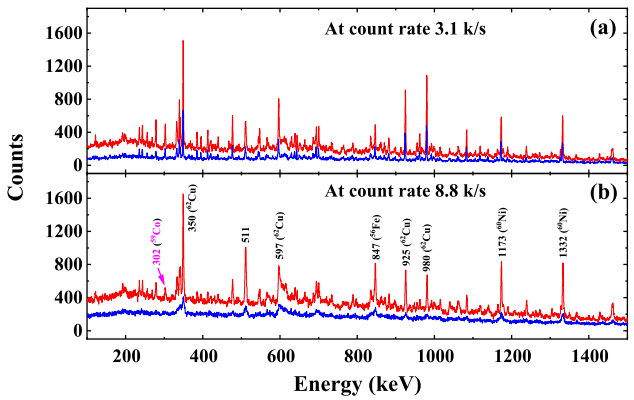

Fig. 5 (Color online) The typical energy spectra of a HPGe detector in the $^{12}C + {}^{54}Cr$ reaction measured by the ADAQ (lower spectrum) and DDAQ (upper spectrum) within the same time range at count rate **a** 3.1 k/s and **b** 8.8 k/s

lead to a certain dead time of the system. In contrast, the DDAQ has nearly no dead time in data transmission and conversion. Therefore, the DDAQ is more efficient in recording data than the ADAQ. At a high count rate, the dead time of the ADAQ becomes serious and acquisition efficiency gets worse. For example, at a trigger rate of 5 k/s, the acquisition efficiency of the ADAQ is only around 67%. Meanwhile, the pile-up also becomes serious at high count rates, which has a significant influence on the spectrum for the ADAQ and little influence on the spectrum for the DDAQ owing to its excellent capability of handling pile-up pulses. Therefore, as shown in Fig. 5b, at a high count rate of 8.8 k/s, compared with the spectrum measured by ADAQ, the spectrum measured by DDAQ has higher data throughput and much better energy resolution. In Fig. 5b, some strong γ-ray transitions in ^{62}Cu, ^{60}Ni, and ^{56}Fe nuclei are clearly seen in the spectrum recorded by DDAQ.

A γ–γ symmetric matrix was built from the coincidence events with a coincident time window of 200 ns. The level scheme analysis was performed using the RADWARE package [27]. To get a clean spectrum, subtractions of random coincidence events from surrounding beam-activated products have been made for the data recorded by the DDAQ. In the ADAQ, the coincident time window of the two detectors was fixed. When the time difference between any two detectors was within the time window, the analog acquisition system was triggered. The coincident time window in ADAQ is usually set to be very small ($\sim$ 200 ns), which is not good for estimating random coincidence events. Since the DDAQ was operated with a triggerless mode and the timestamp of each detector was recorded well, any length of coincidence time window of two detectors can be built in the offline analysis. Figure 6a shows the spectrum of the time difference between detectors for DDAQ. The blue shadow region is the true coincidence, while the red shadow regions can be used to construct the random coincident matrices. By subtracting the random coincident matrices from the γ-coincidence matrix, random coincidence events can be effectively removed. To evaluate the random coincident matrices accurately, ROOT software [28] was also used for cross-checks. Figure 6b and c shows the spectra with the subtractions of random coincidence events. It can be seen that the γ-rays from the ^{197}Au backing are removed effectively.

With higher data throughput and better energy resolution recorded by the DDAQ, as well as the lower interference from the surroundings, weak transitions from nuclei with small cross sections can be observed in the present in-beam measurement. For example, Fig. 7a shows the coincident spectrum gated on the 302-keV γ-ray of the weakly populated ^{59}Co in the $^{12}C + {}^{54}Cr$ reaction. The cascade of ^{59} Co [29, 30] shown in Fig. 7b can be observed in Fig. 7a; in particular, the weak γ-rays of 2652 and 2717 keV are clearly seen in the inset of Fig. 7a, measured by the DDAQ, but not by the ADAQ.

5 Summary

A newly developed DDAQ at Peking University, which is based on Pixie-16 modules from XIA LLC, was tested with the γ-ray detector array of CIAE in comparison with the conventional ADAQ. The measurements with the γ-ray sources indicate that, with careful adjustment of parameters, both the ADAQ and DDAQ exhibit good and comparable energy resolutions at a low counting rate. The in-beam measurements reveal that although at low count

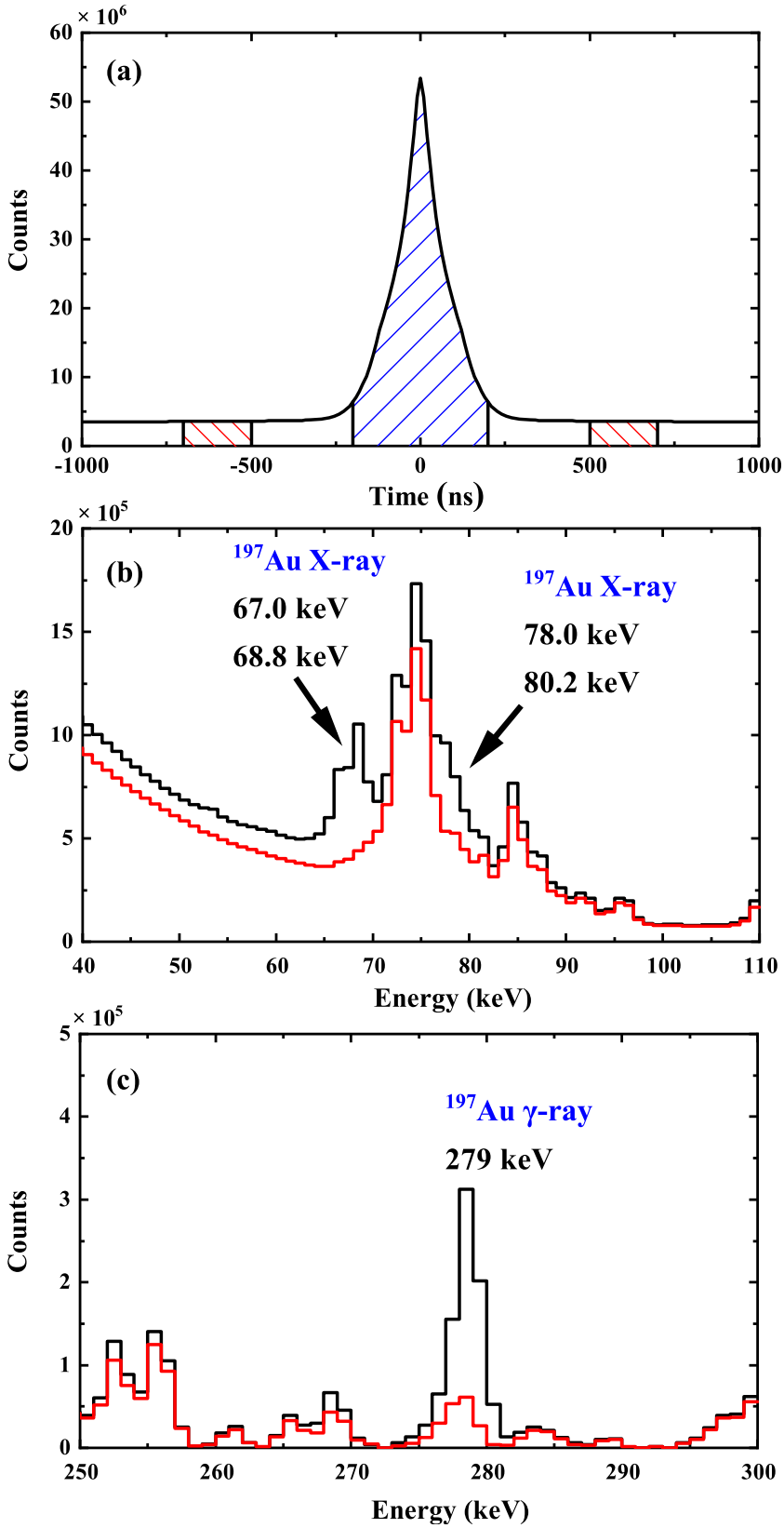

Fig. 6 (Color online) **a** The spectrum of time difference between detectors obtained by the DDAQ. **b** and **c** Total projection spectra with (lower spectra) and without (upper spectra) the subtraction of random coincidence events

rates, both data acquisition systems show energy resolutions similar to the results obtained in the source measurements, at high count rates above 8.8 k/s, the energy resolution obtained by the ADAQ deteriorates significantly

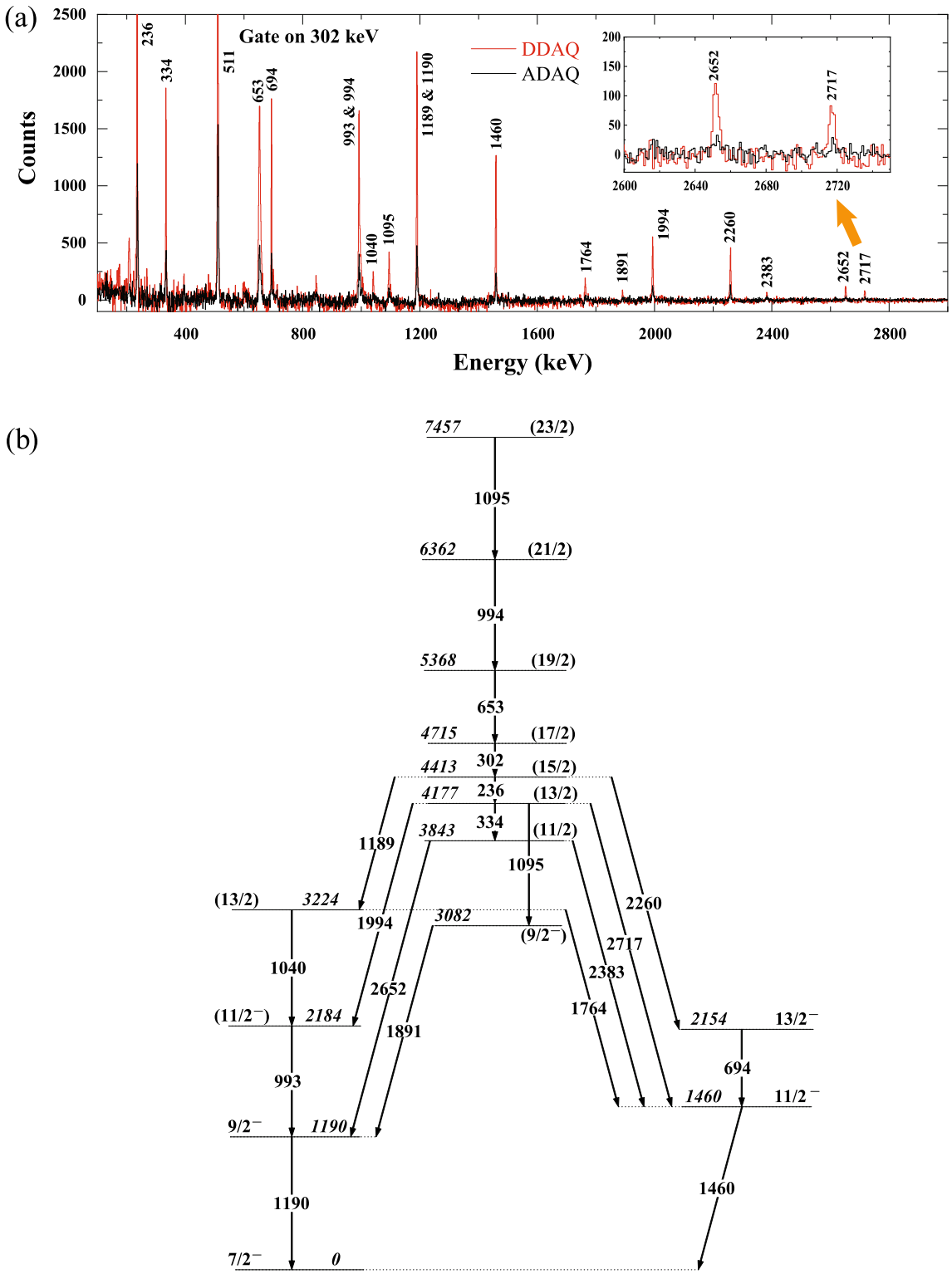

Fig. 7 (Color online) **a** Coincident γ-ray spectrum with gating on the 302-keV transition of ^{59}Co. **b** Partial level scheme of ^{59}Co [29, 30] relevant to the discussion

compared with the almost constant energy resolution obtained by the DDAQ. In addition, under the same experimental conditions, almost twice as many γ-ray coincidence events were collected by the DDAQ compared to the number of coincidence events collected by the ADAQ. The differences in performance between the

ADAQ and DDAQ at high counting rates can be attributed to the DDAQ's excellent capability of handling pile-up pulses at high count rates and the fact that it has nearly no dead time in data transmission and conversion.

The procedures of how the pile-up signal is treated in the DDAQ and ADAQ are described. It is shown that the Gaussian shaping pulse adopted in ADAQ cannot effectively separate the pile-up pulse owing to its long tail, while the trapezoidal shaping pulse of DDAQ, which decays back to baseline very quickly, provides a good identification of the pile-up signal and precisely extracts the energy information of the pile-up signal. Operating with a triggerless mode and recording the timestamp of each detector in the DDAQ, the random coincident events can be subtracted from the γ–γ coincidence matrix. The DDAQ exhibits a clear advance over the conventional ADAQ. This DDAQ has been successfully implemented in γ-spectroscopy experiments at the CIAE and iThemba LABS in South Africa. Benefiting from higher data throughput and better energy resolution, the transitions from weakly populated nuclei can be clearly observed. The experimental results and physical analysis will be presented elsewhere. The flexibility of the DDAQ promotes its wide application in the future nuclear structure research, especially for experiments using not only large HPGe detector arrays but also ancillary detector arrays.

Acknowledgements The authors wish to thank X.G. Wu, Y. Zheng, C.B. Li, H. Tan, and W. Hennig for their great help during testing of this DDAQ.

Author Contributions All authors contributed to the study conception and design. Material preparation, data collection, and analysis were performed by Di-Wen Luo, Hong-Yi Wu, and Zhi-Huan Li. The first draft of the manuscript was written by Di-Wen Luo and all authors commented on previous versions of the manuscript. All authors read and approved the final manuscript.

References

1. J. Eberth, J. Simpson, From Ge(Li) detectors to gamma-ray tracking arrays-50 years of gamma spectroscopy with germanium detectors. Prog. Part. Nucl. Phys. **60**, 283–337 (2008). https://doi.org/10.1016/j.ppnp.2007.09.001
2. M.A. Riley, J. Simpson, E.S. Paul, High resolution gamma-ray spectroscopy and the fascinating angular momentum realm of the atomic nucleus. Phys. Scr. **91**, 123002 (2016). https://doi.org/10.1088/0031-8949/91/12/123002
3. M.J. Koskelo, I.J. Koskelo, B. Sielaff, Comparison of analog and digital signal processing systems using pulsers. Nucl. Instrum. Methods Phys. A **422**, 373–378 (1999). https://doi.org/10.1016/S0168-9002(98)00986-3
4. S. Mitra, L. Wielopolski, G. Hendrey, Comparison of a digital and an analog signal processing system for neutron inelastic gamma-ray spectrometry. Appl. Radiat. Isot. **61**, 1463–1468 (2004). https://doi.org/10.1016/j.apradiso.2004.02.024
5. W.K. Warburton, P.M. Grudberg, Current trends in developing digital signal processing electronics for semiconductor detectors. Nucl. Instrum. Methods Phys. A **568**, 350–358 (2006). https://doi.org/10.1016/j.nima.2006.07.021
6. A. Al-Adili, F.-J. Hambsch, S. Oberstedt et al., Comparison of digital and analogue data acquisition systems for nuclear spectroscopy. Nucl. Instrum. Methods Phys. A **624**, 684–690 (2010). https://doi.org/10.1016/j.nima.2010.09.126
7. P. Wang, R.Y. Zhang, Y.Y. Yan et al., An acquisition system of digital nuclear signal processing for the algorithm development. Nucl. Sci. Tech. **24**, 060408 (2013). https://doi.org/10.13538/j.1001-8042/nst.2013.06.012
8. R.S. Dong, L. Zhao, J.J. Qin et al., Design of a 20-Gsps 12-bit time-interleaved analog-to-digital conversion system. Nucl. Sci. Tech. **32**, 25 (2021). https://doi.org/10.1007/s41365-021-00863-5
9. H.C. Scraggs, C.J. Pearson, G. Hackman et al., TIGRESS highly-segmented high-purity germanium clover detector. Nucl. Instrum. Methods Phys. A **543**, 431–440 (2005). https://doi.org/10.1016/j.nima.2004.12.012
10. J.-P. Martin, C. Mercier, N. Starinski et al., The TIGRESS DAQ/trigger system. IEEE Trans. Nucl. Sci. **55**, 84–90 (2008). https://doi.org/10.1109/TNS.2007.910853
11. M. Descovich, I.Y. Lee, P. Fallon et al., In-beam measurement of the position resolution of a highly segmented coaxial germanium detector. Nucl. Instrum. Methods Phys. A **553**, 535–542 (2005). https://doi.org/10.1016/j.nima.2005.07.016
12. W.F. Mueller, J.A. Church, T. Glasmacher et al., Thirty-two-fold segmented germanium detectors to identify γ-rays from intermediate-energy exotic beams. Nucl. Instrum. Methods Phys. A **466**, 492–498 (2001). https://doi.org/10.1016/S0168-9002(01)00257-1
13. K. Starosta, C. Vaman, D. Miller et al., Digital data acquisition system for experiments with segmented detectors at National Superconducting Cyclotron Laboratory. Nucl. Instrum. Methods Phys. A **610**, 700–709 (2009). https://doi.org/10.1016/j.nima.2009.09.016
14. C.J. Prokop, S.N. Liddick, B.L. Abromeit et al., Digital data acquisition system implementation at the National Superconducting Cyclotron Laboratory. Nucl. Instrum. Methods Phys. A **741**, 163–168 (2014). https://doi.org/10.1016/j.nima.2013.12.044
15. P.-A. Söderström, F. Recchia, J. Nyberg et al., Interaction position resolution simulations and in-beam measurements of the AGATA HPGe detectors. Nucl. Instrum. Methods Phys. A **638**, 96–109 (2011). https://doi.org/10.1016/j.nima.2011.02.089
16. S. Akkoyun, A. Algora, B. Alikhani et al., AGATA-advanced gamma tracking array. Nucl. Instrum. Methods Phys. A **668**, 26–58 (2012). https://doi.org/10.1016/j.nima.2011.11.081
17. R. Palit, S. Saha, J. Sethi et al., A high speed digital data acquisition system for the Indian National gamma array at Tata Institute of Fundamental Research. Nucl. Instrum. Methods Phys. A **680**, 90–96 (2012). https://doi.org/10.1016/j.nima.2012.03.046
18. S. Das, S. Samanta, R. Banik et al., A Compton suppressed detector multiplicity trigger based digital DAQ for gamma-ray spectroscopy Author links open overlay panel. Nucl. Instrum. Methods Phys. A **893**, 138–145 (2018). https://doi.org/10.1016/j.nima.2018.03.035
19. H.Y. Wu, Z.H. Li, H. Tan et al., A general-purpose digital data acquisition system (GDDAQ) at Peking University. Nucl. Instrum. Methods Phys. A **975**, 164200 (2020). https://doi.org/10.1016/j.nima.2020.164200
20. J.G. Wang, S.J. Zhu, L. Gu et al., High-spin states and collective band structures in the odd–odd ^{140}Pm nucleus. J. Phys. G Nucl. Part. **37**, 125107 (2010). https://doi.org/10.1088/0954-3899/37/12/125107
21. XIA LLC, https://xia.com/

22. H. Tan, W. Hennig, M. Walby et al., Digital data acquisition modules for instrumenting large segmented germanium detector arrays, in *2008 IEEE Nuclear Science Symposium Conference Record* (2008), pp. 3196–3200. https://doi.org/10.1109/NSSMIC.2008.4775029
23. W. Hennig, H. Tan, M. Walby et al., Clock and trigger synchronization between several chassis of digital data acquisition modules. Nucl. Instrum. Methods Phys. B **261**, 1000–1004 (2007). https://doi.org/10.1016/j.nimb.2007.04.181
24. S.W. Smith, *The Scientist and Engineer's Guide to Digital Signal Processing*, 2nd edn. (California Technical Publishing, San Diego, 1999), pp. 277–282
25. V.T. Jordanov, G.F. Knoll, Digital synthesis of pulse shapes in real time for high resolution radiation spectroscopy. Nucl. Instrum. Methods Phys. A **345**, 337–345 (1994). https://doi.org/10.1016/0168-9002(94)91011-1
26. V.T. Jordanov, G.F. Knoll, A.C. Hubera et al., Digital techniques for real-time pulse shaping in radiation measurements. Nucl. Instrum. Methods Phys. A **353**, 261–264 (1994). https://doi.org/10.1016/0168-9002(94)91652-7
27. D.C. Radford, ESCL8R and LEVIT8R: Software for interactive graphical analysis of HPGe coincidence data sets. Nucl. Instrum. Methods Phys. A **361**, 297–305 (1995). https://doi.org/10.1016/0168-9002(95)00183-2
28. ROOT Data Analysis Framework, https://root.cern.ch//
29. E.K. Warburton, J.W. Olness, A.M. Nathan et al., Yrast decay schemes from heavy-ion + ^{48}Ca fusion-evaporation reactions. II. $^{59-60}$Fe and $^{59-60}$Co. Phys. Rev. C **16**, 1027–1039 (1977). https://doi.org/10.1103/PhysRevC.16.1027
30. Evaluated Nuclear Structure Data File (ENSDF), http://www.nndc.bnl.gov/ensdf